Acta Crystallographica Section D
Biological Crystallography
ISSN 0907-4449

Pseudo-symmetry and twinning in crystals of homologous antibody Fv fragments

Cory L. Brooks,[a] Ryan J. Blackler,[a] Sandra Gerstenbruch,[b] Paul Kosma,[c] Sven Müller-Loennies,[b] Helmut Brade[b] and Stephen V. Evans[a]*

[a]University of Victoria, Department of Biochemistry and Microbiology, Victoria BC V8P 3P6, Canada, [b]Research Center Borstel, Leibniz Center for Medicine and Biosciences, Department of Biochemical Microbiology Parkallee 22, D-23845 Borstel, Germany, and [c]Department of Chemistry, University of Natural Resources and Applied Life Sciences, A-1190 Vienna, Austria

Correspondence e-mail: svevans@uvic.ca

Received 18 July 2008
Accepted 15 October 2008

PDB References: SAG173-04, 3dur, r3dursf; SAG506-01, 3dv4, r3dv4sf; 3dus, r3dussf; 3dv6, r3dv6sf; 3duu, r3duusf.

A difference of seven conservative amino-acid substitutions between two single-chain antibodies (scFvs) specific for chlamydial lipopolysaccharide does not significantly affect their molecular structures or packing contacts, but dramatically affects their crystallization. The structure of the variable domain (Fv) of SAG173-04 was solved to 1.86 Å resolution and an $R_{\rm cryst}$ of 18.9% in space group $P2_12_12_1$. Crystals of the homologous SAG506-01 diffracted to 1.95 Å resolution and appeared at first to have Patterson symmetry $I4/m$ or $P4/mmm$; however, no solution could be found in space groups belonging to the former and refinement in the only solution corresponding to the latter (in space group $P4_32_12$) stalled at $R_{\rm free}$ = 30.0%. Detailed examination of the diffraction data revealed that the crystal was likely to be twinned and that the correct space group was $P2_12_12_1$. Both translational pseudo-symmetry and pseudo-merohedral twinning were observed in one crystal of SAG506-01 and pseudo-merohedral twinning was observed for a second crystal. The final R factor for SAG506-01 after refinement in $P2_12_12_1$ was 20.5%.

1. Introduction

Twinning is a crystal-growth pathology in which the crystal is composed of two or more domains whose lattices differ in their respective orientation (Koch, 1992). In epitaxial twinning the separate crystal lattices do not superimpose in three dimensions, which is apparent in the diffraction pattern (Yeates & Fam, 1999). In the case of merohedral twinning the twin domains are superimposable in three dimensions and thus are not evidenced in the diffraction pattern (Yeates & Fam, 1999; Yeates, 1997). This form of twinning is typically observed in a limited set of high-symmetry space groups in the tetragonal, trigonal, hexagonal and cubic systems (Yeates & Fam, 1999; Yeates, 1997). Although true merohedral twinning can only occur in a high-symmetry space group, pseudo-merohedral twinning can occur under special conditions with monoclinic and orthorhombic systems that display pseudo-symmetry in their unit-cell dimensions, which can cause difficulties in proper space-group assignment and structure determination. For example, pseudo-merohedral twinning in a monoclinic space group with $\beta \simeq 90^\circ$ can mimic an orthorhombic space group, while pseudo-merohedral twinning in an orthorhombic space group with $a \simeq b$ can mimic a tetragonal space group.

A consequence of the superposition of the direct lattices in pseudo-merohedral twinning is the superimposition of their reciprocal lattices, where each reflection becomes a weighted sum of the distinct reflections from the separate twin domains.

Merohedral and pseudo-merohedral twinning lead to predictable deviations in intensity statistics and twinning can be detected by anomalies in the observed cumulative intensity distribution from Wilson statistics (Chandra *et al.*, 1999; Stanley, 1972; Wilson, 1949).

The bacterial family Chlamydiaceae is comprised of two genera, *Chlamydia* (*C.*) and *Chlamydophila* (*Cp.*), with a total of four species, *Cp. psittaci*, *C. trachomatis*, *Cp. pneumoniae* and *C. pecorum*, all of which are pathogenic and obligatory intracellular bacteria that cause a variety of diseases in both animals and humans. Antibodies against specific carbohydrate structures located in the lipopolysaccharide (LPS) play an important role in the clinical diagnosis of chlamydial diseases in human and veterinary medicine (Bowie *et al.*, 1990). The LPS of Chlamydiaceae has been well characterized (Kosma, 1999) and contains a unique (family-specific) trisaccharide epitope composed of 2,8–2,4-linked residues of 3-deoxy-α-D-*manno*-oct-2-ulosonic acid (Kdo; Fig. 1*a*). In addition, the LPS of *Cp. psittaci* contains a 2,4–2,4-linked Kdo trisaccharide and a branched Kdo tetrasaccharide (Fig. 1*b*). With the aim of differentiating *Cp. psittaci* from the other species using monoclonal antibodies (mAbs), we have generated various clones by conventional hybridoma techniques that allow differentiation to a greater or lesser extent. However, these clones were unable to distinguish between the 2,4–2,4-linked trisaccharide and the branched tetrasaccharide (Fig. 1*c*; Müller-Loennies *et al.*, 2006; Nguyen *et al.*, 2003).

Using phage-display methods, we have now generated two high-affinity single-chain fragments (scFv) labelled SAG506-01 and SAG173-04. These scFvs differ by seven amino acids, most of which are conservative substitutions (Fig. 2). The higher ability of these two scFvs to discriminate between these linkages is primarily the consequence of a single amino-acid substitution in CDR H3 (h99Ala→h99Val; Müller-Loennies *et al.*, unpublished data). Here, we describe the crystallization and structure determination of these scFv fragments.

2. Materials and methods

2.1. Production and purification of recombinant ScFv fragments

Both scFvs were expressed in 5 × 2 l cultures of *Escherichia coli* TG-1 grown in 5 l Erlenmeyer flasks from plasmid pSJF8 as described previously (Müller-Loennies *et al.*, 2006). Soluble scFv was extracted from the periplasm of pelleted cells using polymyxin B (Müller-Loennies *et al.*, 2006) and was precipitated by the addition of 50%(*w*/*v*) ammonium sulfate. Both scFvs were also obtained from culture supernatants by ammonium sulfate precipitation. Ammonium sulfate precipitates were centrifuged (10 000*g*), resuspended in 50 m*M* NaH_2PO_4, 0.3 *M* NaCl pH 8.0 and centrifuged again (10 000*g*) to remove insoluble material. The supernatant was applied onto an Ni-Sepharose column (GE Healthcare) and the column was washed with 50 m*M* NaH_2PO_4, 0.3 *M* NaCl, 10 m*M* imidazole pH 8.0 and then with 50 m*M* NaH_2PO_4, 0.3 *M* NaCl, 20 m*M* imidazole pH 8.0. The scFvs were then eluted with 50 m*M* NaH_2PO_4, 0.3 *M* NaCl, 0.3 *M* imidazole pH 8.0 and dialyzed into phosphate-buffered saline pH 7.4.

2.2. Generation of Fv fragments for crystallization

Intact scFvs are frequently not amenable to crystallization because of their propensity to form higher order oligomers

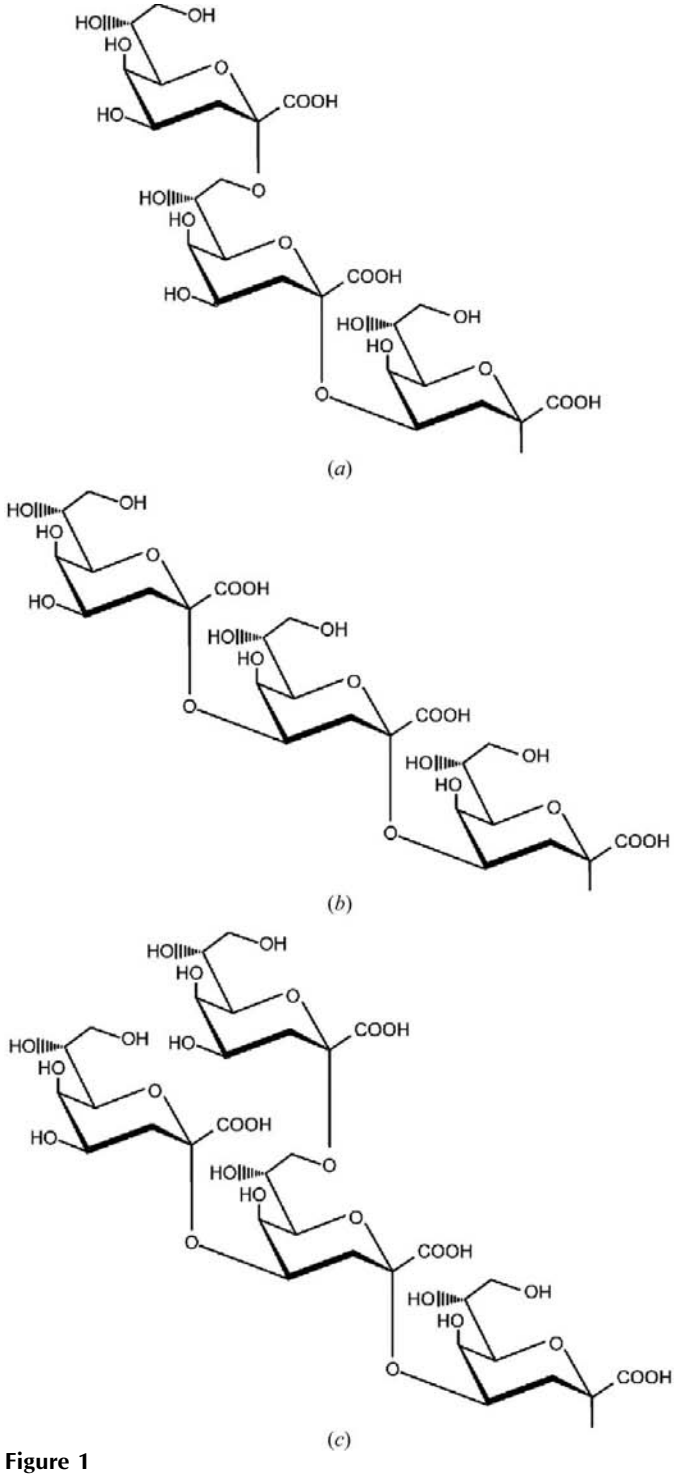

Figure 1
Chemical structure of chlamydial LPS. All chlamydial species investigated so far contain the 2,8–2,4-linked Kdo trisaccharide shown in (*a*). Kdo-(2,4)-Kdo-(2,4)-Kdo (*b*) and Kdo(2,8)-[Kdo(2,4)]-Kdo-(2,4)-Kdo-(2,4) (*c*) occur only in *Cp. psittaci*.

Table 1
Crystallographic data collection and structure refinement.

	SAG173-04	SAG506-01 crystal 1			SAG506-01 crystal 2	
	Orthorhombic	Tetragonal, pseudo-centred	Tetragonal	Orthorhombic	Tetragonal	Orthorhombic
Data collection						
Wavelength	1.5418	1.5418	1.5418	1.5418	1.5418	1.5418
Resolution range (Å)	19.90–1.86 (1.93–1.86)	19.96–2.60 (2.69–2.60)	19.81–1.95 (2.02–1.95)	19.81–1.95 (2.02–1.95)	19.89–1.95 (2.02–1.95)	19.89–1.95 (2.02–1.95)
Patterson group	*Pmmm*	*I*4/*m*	*P*4/*mmm*	*Pmmm*	*P*4/*mmm*	*Pmmm*
Space group	$P2_12_12_1$		$P4_32_12$	$P2_12_12_1$	$P4_32_12$	$P2_12_12_1$
Unit-cell parameters						
a (Å)	70.76	145.13	72.51	72.47	71.42	71.60
b (Å)	72.19			72.56		71.76
c (Å)	85.13	171.92	85.91	85.91	86.08	86.21
Z	2		1	2	1	2
Unique reflections	35356	28445	17255	33108	21349	32545
R_{merge} (%)	9.2	9.7 (25.8)	7.0 (42.5)	6.5 (38.0)	7.2	6.7
$I/\sigma(I)$	9.1 (3.9)	12.3 (7.1)	14.7 (4.4)	11.7 (3.6)	15.7 (5.7)	11.4 (3.6)
Redundancy	4.68 (4.38)	17.1 (17.1)	9.40 (9.11)	4.90 (4.85)	8.88 (8.36)	4.65 (4.48)
Completeness (%)	94.9 (98.2)	100 (100)	99.9 (99.8)	98.4 (95.6)	99.7 (96.7)	98.6 (99.9)
Refinement						
R_{cryst} (R_{free})	17.81 (24.65)		26.92 (33.58)	25.27 (28.15)	22.93 (30.34)	19.37 (21.69)
Twin fraction (α)				0.5		0.493
R.m.s. deviations from ideality						
Bonds	0.017		0.003	0.002	0.005	0.006
Angles	1.821		0.614	0.506	1.029	1.040
Dihedrals	19.5		16.049	15.558	20.241	18.734
Ramachandran plot						
Most favourable (%)	90.5		87.8	84.9	87.9	83.5
Allowed (%)	8.8		10.7	13.8	11.1	15.4
Generously allowed (%)	0.3		1.0	0.8	0.5	0.5
Disallowed (%)	0.5		0.5	0.5	0.5	0.5
PDB code	3dur		3dv4	3dus	3dv6	3duu

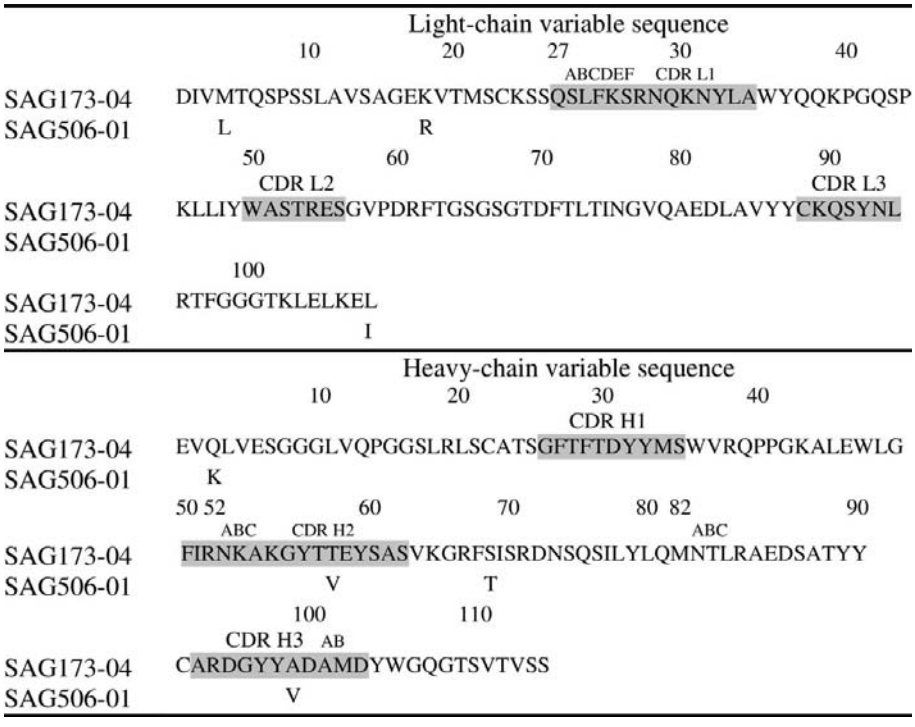

Figure 2
Amino-acid sequence of the variable regions of SAG173-04 and SAG506-01. There are a total of three amino-acid differences in the two variable light-chain regions and four amino-acid differences in the two heavy-chain variable regions; however, only one of these differences lies in the hypervariable regions that potentially contact the antigen. The amino-acid sequence is numbered according to the Kabat numbering scheme (Kabat *et al.*, 1991). CDRs are indicated by grey shading.

(Essig *et al.*, 1993). In order to produce monomeric scFv fragments, the linker peptides of the scFv fragments of SAG173-04 and SAG506-01 were digested with subtilisin (Sigma) using a 1:1000(*w*:*w*) ratio at room temperature and quenched with 1 m*M* phenylmethylsulfonyl fluoride (Sigma). Optimal digestion times and protease:scFv ratios were determined by SDS–PAGE analysis (15%). After digestion, the scFvs were dialyzed into 20 m*M* HEPES pH 7.5 and concentrated to 10 mg ml^{-1}.

2.3. Crystallization of Fv fragments

The ScFv fragments of SAG506-01 and SAG173-04 were mixed with Kdo (60 m*M*; Toronto Research Chemicals) and screened using Crystal Screen I (Hampton Research) by hanging-drop vapour diffusion. Preliminary crystals appeared after 3 d in well 6 (0.1 *M* Tris pH 8.5, 0.2 *M* $MgCl_2$, 30% PEG 4000). Diffraction-quality crystals of both SAG506-01 and SAG173-04 were obtained using a concentration of

15 mg ml^{-1} in 60 m*M* Tris pH 8.0, 0.13 *M* $MgCl_2$, 20% PEG 4000.

2.4. Data collection, structure determination and refinement

Crystals were flash-frozen to 113 K using an Oxford Cryostream 700 crystal cooler (Oxford Cryosystems) using mother liquor supplemented with 25% MPD as a cryoprotectant. Data were collected on a Rigaku R-AXIS IV^{++} area detector (Rigaku, Japan) coupled to a MM-002 X-ray generator with Osmic Blue optics (Rigaku Americas, Texas) and were processed using *CrystalClear*/*d*TREK* (Rigaku). The structure of SAG173-04 was solved by molecular replacement using *Phaser* (Storoni *et al.*, 2004), with the variable domain of the homologous antibody S45-18 (PDB code 1q9w) as a search model. Manual fitting of σ_A-weighted $F_o - F_c$ and $2F_o - F_c$ electron-density maps was carried out with *Coot* (Emsley & Cowtan, 2004) and *SetoRibbon* (Evans, unpublished program). Restrained refinements were carried out with *REFMAC*5, as implemented in *CCP*4 (Collaborative Computational Project, Number 4, 1994). Final model and refinement statistics are give in Table 1. The structure of SAG506-01 was solved by molecular replacement using *Phaser* (Storoni *et al.*, 2004), with the structure of SAG173-04 as a search model and with refinement and fitting carried out as for SAG173-04. *phenix.xtriage* was used to test for pseudo-merohedral twinning and *phenix.refine* was used to refine twinned data, as implemented in *PHENIX* (Adams *et al.*, 2002). Final model and refinement statistics are give in Table 1.

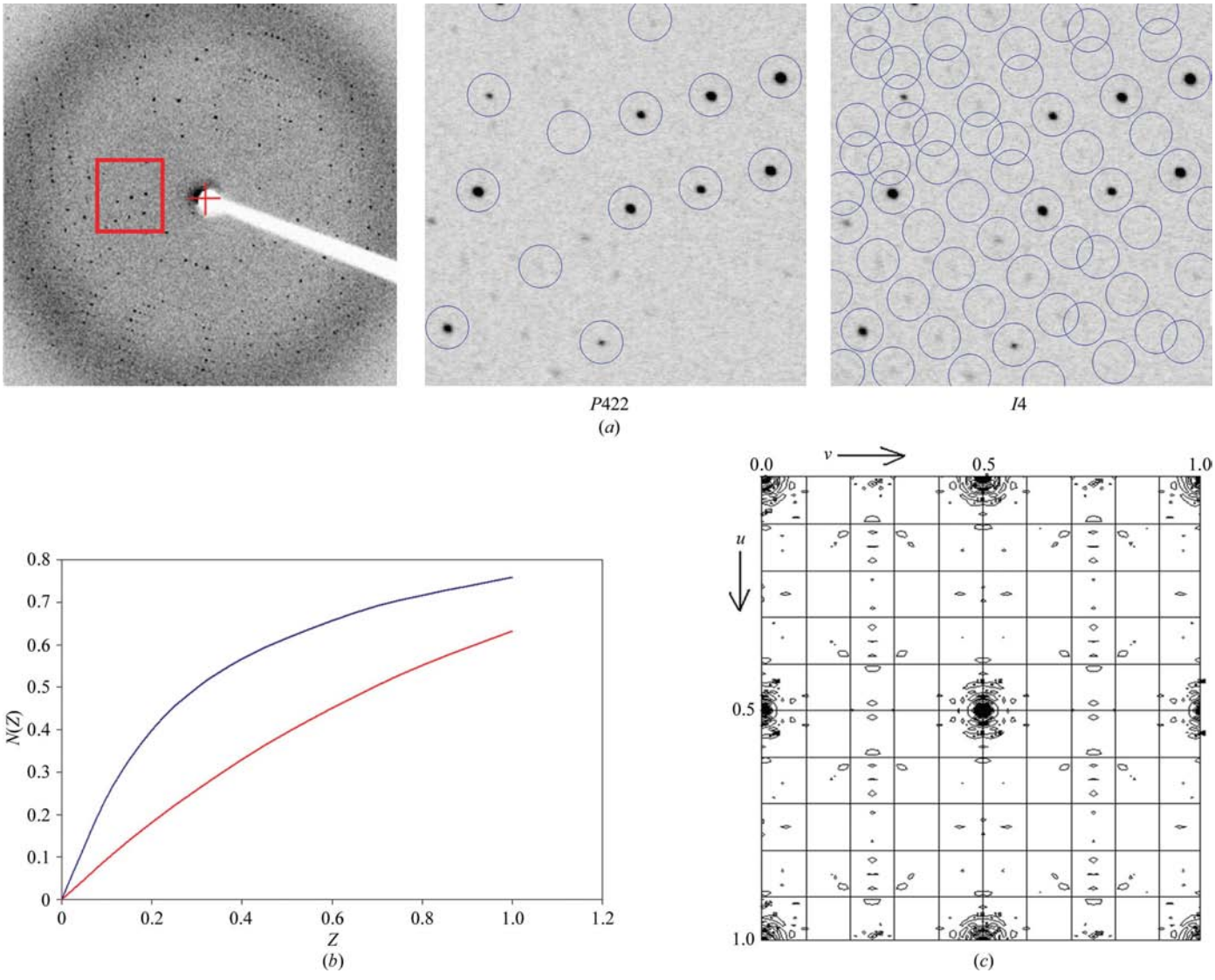

Figure 3
Detection of crystal pathologies in SAG506-01. (*a*) The diffraction pattern of liganded SAG506-01 does not exhibit the split spots characteristic of epitaxial twinning. Spot predictions for both *P*422 and *I*4 are shown. The weak *h* odd, *k* odd and *l* odd reflections found in space group *I*4 are a consequence of the presence of pseudo-translational symmetry. (*b*) Cumulative intensity distribution $N(Z)$ of acentric reflections of SAG506-01 crystal 1. The observed values (blue lines) are significantly greater than the theoretical values (red lines), indicating the presence of pseudo-translational symmetry. Cumulative intensity distribution curves were calculated with *phenix.xtriage* as implemented in *PHENIX* (Adams *et al.*, 2002). (*c*) Patterson map of reflection data of SAG506-01. The large off-origin peaks halfway along each axis indicate the presence of pseudo-translational symmetry.

3. Results and discussion

3.1. Translational pseudo-symmetry and ambiguity in space-group assignment

Crystals of the homologous Fv fragments of SAG173-04 and SAG506-01 grew under identical conditions, yet the crystals exhibited different morphologies. The structure of SAG173-04 was solved in space group $P2_12_12_1$, with the final model giving good stereochemistry and R factors that were comparable with those of other scFv structures (Table 1). Initial reduction of the data collected from crystals of SAG506-01 suggested higher symmetry than SAG173-04, with Patterson symmetry $I4/m$, unit-cell axes approximately double those of SAG173-04 and an $R_{\rm merge}$ of 9.7% (Table 1). All attempts to solve the structure of SAG506-01 by molecular replacement using SAG173-04 as a search model failed, although a partial solu-

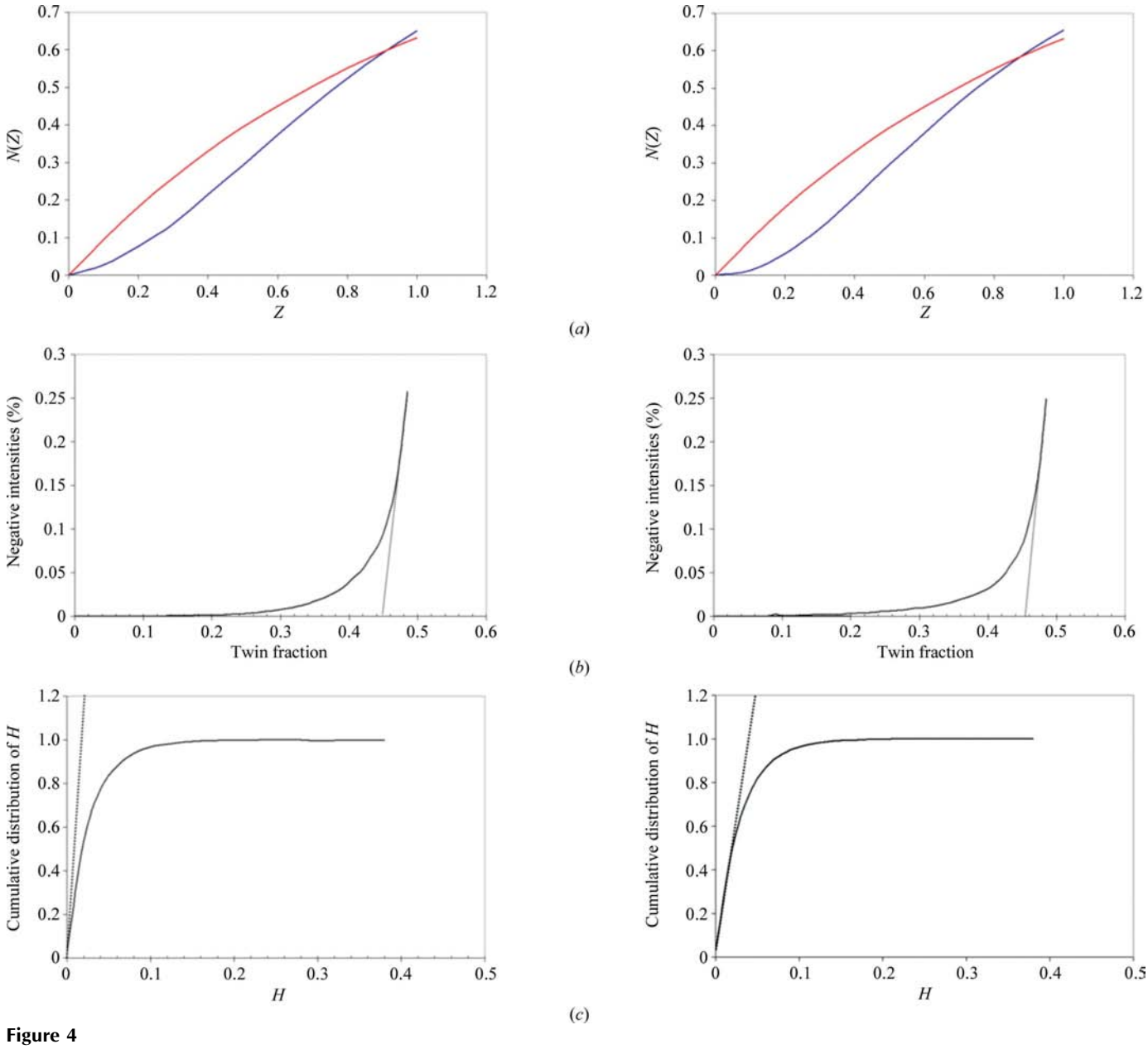

Figure 4
Detection and estimation of the twinning fraction in SAG506-01 crystal 1 (left) and crystal 2 (right) both reduced in the Patterson group $P4/mmm$. (*a*) The $N(Z)$ plot of acentric reflections of SAG506-01 shows that the observed values (blue lines) are lower than the theoretical values (red lines) and sigmoidal, indicating the presence of twinning. (*b*) Estimate of the twinning fraction using the Britton plot (Britton, 1972). The percentage of negative intensities after detwinning is plotted as a function of the assumed value of the twin fraction (α). Overestimating the value of α results in an increase in the negative intensities. The true value of α can then be estimated from this increase. The twin fraction was estimated from where the dotted line intersects the x axis and was estimated to be 0.442 for crystal 1 (left) and 0.445 for crystal 2 (right). (*c*) Estimate of the twinning fraction using the H plot (Yeates, 1988). The cumulative fractional intensity difference of acentric twin-related intensities, $H = |I_1 - I_2|/(I_1 + I_2)$, is plotted as a function of H. The twin fraction is estimated from the initial slope of this intensity distribution (dotted line) and was estimated to be 0.478 for crystal 1 (left) and 0.477 for crystal 2 (right). The cumulative intensity distribution, Britton and H plots were all calculated using *phenix.xtriage* as implemented in *PHENIX* (Adams *et al.*, 2002).

tion was developed (six of eight molecules expected in the asymmetric unit in space group $I4_1$) that defied refinement.

There are several crystal pathologies that have been reported to lead to difficulty in structure solution: translational pseudo-symmetry, epitaxial twinning and merohedral twinning can all cause molecular replacement to fail. In epitaxial twinning the separate crystal lattices and their corresponding diffraction patterns do not superimpose in three dimensions (Yeates & Fam, 1999); however, the diffraction pattern of SAG506-01 showed no indication of multiple lattices (Fig. 3*a*).

An indicator of merohedral twinning is the deviation of the cumulative intensity distribution $N(Z)$ from theoretically calculated values (Chandra *et al.*, 1999; Stanley, 1972; Wilson, 1949). In the case of twinning, the $N(Z)$ curve is expected to have a sigmoidal shape and to be below that of the theoretical values; however, in the case of SAG506-01 the $N(Z)$ distribution was significantly above the expected values (Fig. 3*b*). This kind of $N(Z)$ distribution can be characteristic of pseudo-translational symmetry, which can lead to incorrect assignment of both the unit cell and the space group and mask the effects of twinning on the cumulative intensity distribution curve (Padilla & Yeates, 2003; Lee *et al.*, 2003; Chook *et al.*, 1998). The presence of pseudo-translational symmetry can be confirmed by the presence of a large off-origin peak in the native Patterson map (Zwart *et al.*, 2005).

Examination of the Patterson map of SAG506-01 with Patterson symmetry *I*4/*m* revealed large off-origin peaks at (0.5, 0, 0), (0, 0.5, 0), (0, 0, 0.5) and (0, 0.5, 0.5) with heights ∼85% of the origin (Fig. 3*c*), which is a strong indication of pseudo-translational symmetry on all three axes that leads to an incorrect choice of both space group and unit cell. The Patterson map suggests that the true unit-cell lengths should be halved to $a = b = 72.51$, $c = 85.91$ Å with Patterson symmetry *P*4/*mmm* if the pseudo-translational symmetry was crystallographic. Given the general weakness of *h* odd, *k* odd and *l* odd reflections, the raw data were re-indexed using a 10σ threshold to yield a unit cell with Patterson symmetry *P*4/*mmm* with dimensions half those of the original cell on each axis and similar to those of SAG173-04 (Table 1).

The data were rescaled and averaged with an $R_{\rm merge}$ of 7.0% (Table 1) and solved in $P4_32_12$ using SAG173-04 as a search model. However, after manual model building and refinement the $R_{\rm free}$ stalled at 33%. Another data set was collected from a second crystal of SAG506-01 using a crystal from a different drop (Table 1). The Patterson map of this crystal gave no indication of pseudo-translational symmetry and it was again reduced with Patterson symmetry *P*4/*mmm* with a reasonable value of $R_{\rm merge}$ of 7.2% (Table 1). However, although the structure was solved in space group $P4_32_12$, the refinement

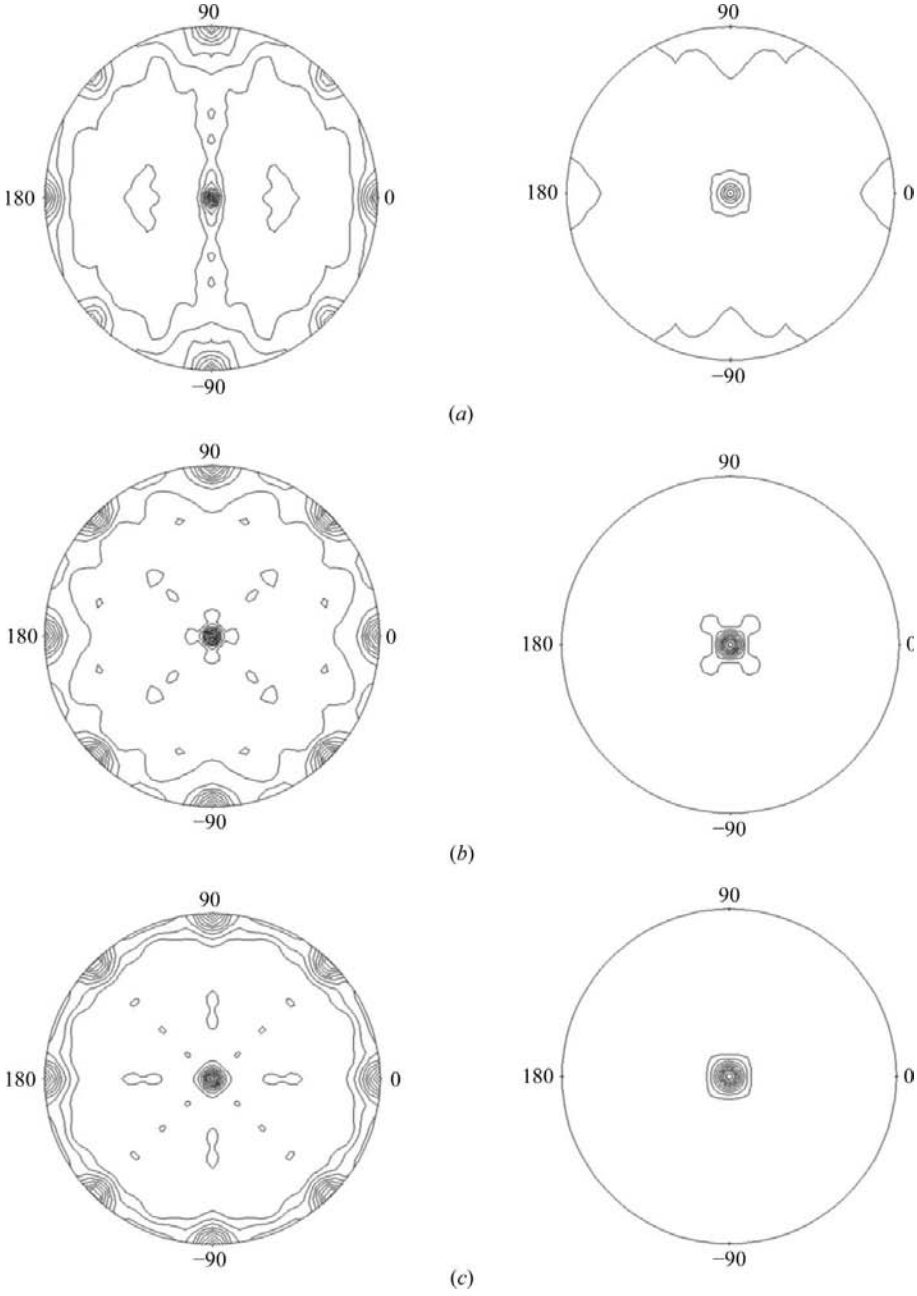

Figure 5
Self-rotation functions at $\kappa = 180^\circ$ (left) and $\kappa = 90^\circ$ (right) showing pseudo-4/*mmm* symmetry owing to NCS in (*a*) crystals of SAG173-04, (*b*) SAG506-01 crystal 1 and (*c*) SAG506-01 crystal 2. Self-rotation functions were calculated using *POLARRFN* as implemented in *CCP*4 (Collaborative Computational Project, Number 4, 1994).

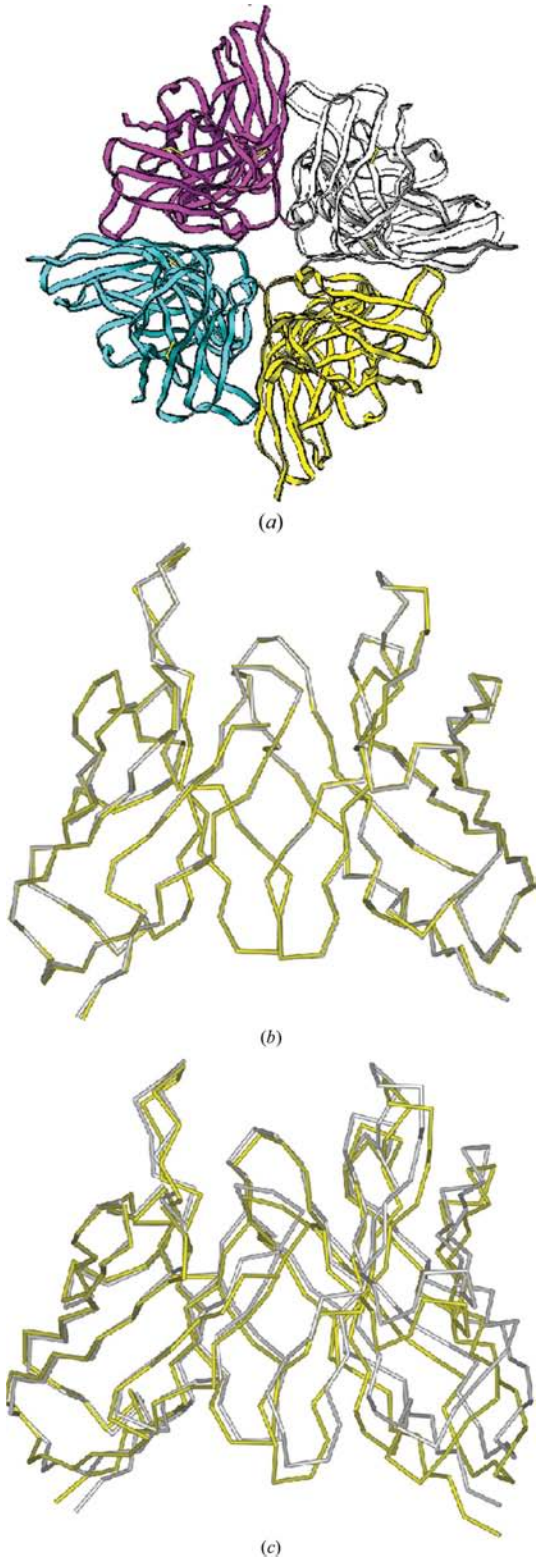

Figure 6
A near-perfect noncrystallographic symmetry operator in SAG506-01 leads to crystal twinning. (*a*) Pseudo-fourfold symmetry in twinned crystals of SAG506-01. (*b*) Application of the NCS operator $(-\frac{1}{4} + y, \frac{1}{4} - x, \frac{1}{4} + z)$ to superpose the first molecule in the asymmetric (white) unit upon the second (yellow) shows that the packing in SAG506-01 is a nearly perfect 4_3 axis. (*c*) Similar application of the same operator in SAG173-04 shows that the same NCS operator cannot accurately represent the crystal packing and explains why this Fv is not susceptible to twinning.

again stalled at an unacceptably high value of $R_{\rm free}$ of 30% (Table 1).

Given the similarity between the *a* and *b* unit-cell lengths and given that the scFv from the related antibody SAG173-04 had a similar unit cell but was solved in space group $P2_12_12_1$, twinning was considered as a second pathology in these crystals. The data were examined for statistical evidence of pseudo-merohedral twinning as a possible explanation for the problems encountered during refinement.

3.2. Detection and treatment of twinned data

Twinning can be detected by several methods, all of which are based upon the examination of intensity statistics (Padilla & Yeates, 2003; Yeates, 1997; Gomis-Rüth *et al.*, 1995; Rees, 1980). One indication of the presence of twinning can be garnered from examination of the theoretical *versus* observed cumulative intensity distribution $N(Z) = f(Z)$, which will be sigmoidal in the case of merohedrally twinned data (Rees, 1980; Gomis-Rüth *et al.*, 1995). The cumulative intensity distribution curve of SAG506-01 was calculated using *phenix.xtriage* (Adams *et al.*, 2002). For both crystals, the $N(Z)$ distribution was below the theoretical values and was found to be sigmoidal in shape, suggesting the presence of twinning (Fig. 4).

Twinning can also be detected by analysis of the second moment of intensities of acentric data (Yeates, 1997). A value of 2.0 is expected for data from an untwinned crystal, while a value of 1.5 is expected in the case of data from a twinned crystal. The first crystal had an $\langle I^2\rangle/\langle I\rangle^2$ of 1.62, while the second crystal had a $\langle I^2\rangle/\langle I\rangle^2$ of 1.79, which suggested the presence of twinning. The standard $\langle I^2\rangle/\langle I\rangle^2$ test can behave anomalously in the presence of anisotropy, pseudo-centering and pseudo-noncrystallographic symmetry. A more robust test developed by Padilla & Yeates (2003) is the *L*-test, which is based upon deviations in local intensities. In the case of no twinning values of 1/2 and 1/3 are expected for the mean $|L|$ and for mean L^2, respectively, while in the case of perfect twinning values of 3/8 and 1/5 are expected. The first crystal of SAG506-01 had a mean $|L|$ of 0.351 and an L^2 of 0.190, while the second had a mean $|L|$ of 0.372 and an L^2 of 0.172, suggesting nearly perfect twinning for both crystals of SAG506-01. The cystals of SAG173-04 had a mean $|L|$ of 0.472 and an L^2 of 0.305, which indicated that no significant twin fraction was present. Another indicator is the multivariate *Z* score, which is a quality measure of the spread of the intensities. Good-quality data have a *Z* score of 3.5 or lower, while large values can be an indication of twinning. The data from SAG173-01 had a *Z* score of 2.7, indicating good-quality data, while the crystals of SAG506-04 had *Z* scores of 4.9 and 5.7 for the first and second crystals, respectively, again consistent with the presence of twinning in SAG506-01.

Since pseudo-merohedral twinning can occur in the orthorhombic system when $a \simeq b$ to yield higher apparent symmetry, the data were reduced in space group $P2_12_12_1$ ($R_{\rm merge}$ = 6.5%) and the structure was solved by molecular replacement to yield two molecules in the asymmetric unit

(Table 1) in the same approximate positions and orientations as the scFv from the related antibody SAG173-04. The twin law that related Patterson symmetry *Pmmm* with *P*4/*mmm* was (k, $-h$, l) and the twin fraction (α) was estimated from the Britton plot (Britton, 1972) and the *H* plot (Yeates, 1988) for data from both crystals of SAG506-01 (Figs. 4*b* and 4*c*). Both crystals exhibited nearly perfect twinning, with estimated twin fractions of 0.442 and 0.445 from the Britton plot (Fig. 4*b*), and estimated twin fractions of 0.478 and 0.477 from the *H* plot (Fig. 4*c*).

Twinned refinement resulted in a substantial improvement in $R_{\rm free}$ in both data sets (Table 1), with $R_{\rm free}$ falling from 33 and 30% to 28.2 and 22.0%, respectively. The final twin fraction refined to 0.5 for the first data set and 0.493 for the second data set (Table 1).

3.3. Noncrystallographic symmetry, pseudo-symmetry and twinning

The presence of noncrystallographic symmetry has been suggested to promote the growth of twinned crystals when the NCS operator corresponds to the twinning operator (MacRae & Doudna, 2007; Larsen *et al.*, 2002; Declercq & Evrard, 2001; Frazão *et al.*, 1999; Liang *et al.*, 1996; Rees & Lipscomb, 1980). Calculation of the self-rotation function for both the untwinned SAG173-04 and the twinned SAG506-01 indicates the presence of pseudo-*P*4/*mmm* symmetry owing to the presence of NCS (Fig. 5). Thus, the twinning which occurred in crystals of SAG506-01 appears to be similar to the twinning that occurred in crystals of a rubredoxin oxygen oxidoreductase (Frazão *et al.*, 1999), where the presence of an NCS twofold axis associates with the crystallographic symmetry to form a fourfold noncrystallographic symmetry axis parallel to *c* (Fig. 6*a*). This phenomenon is known as rotational pseudo-symmetry (RPS) and can occur in cases where the point-group symmetry of the lattice is higher than the point-group symmetry of the crystal (Zwart *et al.*, 2008). RPS (and twinning combined with RPS) can be detected by comparing the *R* factor between reflections related by a twinning operator ($R_{\rm twin}$) for both observed and calculated data (Lebedev *et al.*, 2006). In the cases where both RPS and perfect twinning occur, it is expected that $R_{\rm twin}$ (observed) will be approximately zero and $R_{\rm twin}$ (calculated) will be less than 0.5 (Lebedev *et al.*, 2006). $R_{\rm twin}$ (calculated) for the crystals of SAG506 was 0.25 and 0.308 for the first and second crystals, respectively, while $R_{\rm twin}$ (observed) was 0.043 and 0.042 for the first and second crystals, respectively, thus indicating the presence of both twinning and RPS.

One of the most interesting questions is why is no twinning observed in SAG173-04 despite the nearly identical NCS elements? Comparison of the NCS operators derived from the twinned crystal of SAG506-01 and the nontwinned crystal of SAG173-04 reveals that the NCS operator for the twinned crystal is nearly identical to a 4_3 screw-axis operator ($-\frac{1}{4}+y$, $-\frac{1}{4}-x$, $\frac{1}{4}+z$). This results in nearly perfect superimposition of the two molecules in the asymmetric unit in the twinned crystal (Fig. 6*b*; r.m.s. = 0.28 Å), but imperfect superimposition of these molecules in the nontwinned crystal (Fig. 6*c*; r.m.s. = 0.52 Å). This slight difference in the NCS operators between the twinned and nontwinned crystals provides a mechanism whereby the twin domain forms in the case of SAG506-01 but no twinning is present in SAG173-04.

The few relatively conserved amino-acid substitutions between the two proteins results in only slight differences between the two structures (Fig. 7; r.m.s. = 0.78 Å). The seven substituted amino acids are scattered throughout the protein structure, with three in the light chain and four in the heavy chain (Figs. 1 and 7). Most of the amino-acid substitutions are surface-exposed, with the exception of residues hMet4 (untwinned)→hLeu4 (twinned) and hAla99 (untwinned)→hVal99 (twinned), for which the side chains are buried in the structure. One of the mutations at the C-terminus of the light chain, l108Leu (untwinned)→l108Glu (twinned), was disordered in both of the structures. The mutations only cause subtle perturbations in the structure, which are not confined to the vicinity of the mutations but are rather propagated through different regions in the structure; the largest changes are observed in the heavy chains (Fig. 7), which in turn lead to altered packing interactions between the structures.

In the untwinned structure lLys18 forms a hydrogen bond to lLys23 in the symmetry-related molecule ($-x$, $\frac{1}{2}-y$, $\frac{1}{2}-z$) and hSer68 forms contacts to hSer70 in the symmetry-related molecule ($-x$, $-\frac{1}{2}-y$, $\frac{1}{2}-z$) and to hArg19 in the symmetry-related molecule ($-x$, $\frac{1}{2}-y$, $\frac{1}{2}-z$). In the case of the twinned structure, the packing interaction with residue h18 is lost because the larger Arg residue in the twinned structure has caused lLys23 in the symmetry-related molecule ($-x$, $\frac{1}{2}-y$, $\frac{1}{2}-z$) to move away. The other crystal contacts to hSer70 and hArg19 are maintained to residue Thr68 in the twinned structure; however, an additional crystal contact is formed from hThr68 to hSer70 in the symmetry-related molecule ($-x$, $\frac{1}{2}-y$, $\frac{1}{2}-z$).

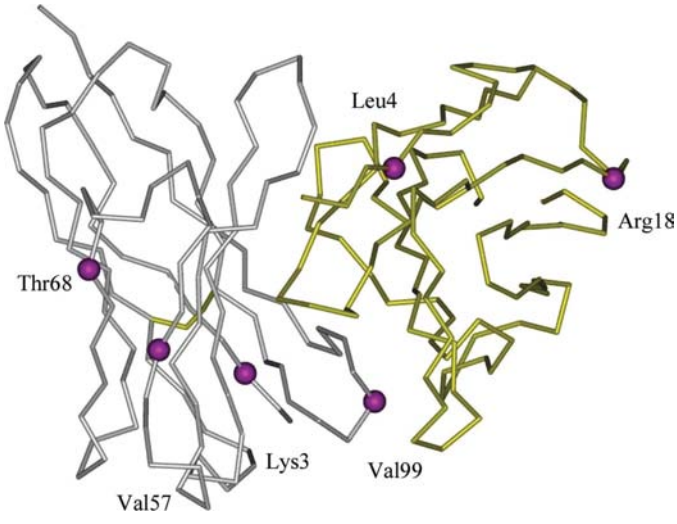

Figure 7
Positions of amino-acid differences between SAG506-01 and SAG173-04. The magenta spheres represent the locations of the amino-acid differences, with the light chain in yellow and the heavy chain in white. A single molecule within the asymmetric unit of SAG506-01 is shown alone for clarity.

Since the slight differences in the structure are not confined to the region surrounding the amino-acid substitutions, the global symmetry contacts between the two structures that govern crystallization are subtly different.

3.4. Mutation represents a new condition for inducing twinning

Twin-domain growth in a crystal will only be observed if the intermolecular interactions across a twin boundary are energetically favourable compared with the formation of a single crystal (Parsons, 2003), indicating that the amino-acid substitutions in SAG506-01 may change the energetic balance between the formation of a twin domain and the formation of a single crystal for these two homologous antibodies. Thus, point mutations can be added to the phenomena previously observed to lead to twinning, such as heavy-metal soaking, ligand binding, selenomethionine substitution and cryo-induced condensation (Helliwell *et al.*, 2006; Parsons, 2003; Poulsen *et al.*, 2001; Herbst-Irmer & Sheldrick, 1998).

4. Conclusions

The structure determination of SAG173-04 and SAG506-01 represents an interesting case where a small number of amino-acid substitutions results in the presence of crystal-growth pathologies in the crystals of SAG506-01. Examination of a Patterson map suggested the presence of pseudo-centring, which eventually allowed the selection of the correct unit cell. The resultant solution gave strong indications of twinning and twinned refinement resulted in dramatic improvements in the *R* factors. Although nearly identical in structure, the slight difference arising from a few amino-acid substitutions resulted in nontwinned crystals of SAG173-04 and twinned crystals of SAG506-01. The formation of the twin domain in the case of SAG506-01 may arise from the presence of a near-perfect tetragonal NCS operator which may have permitted the growth of the twin domain.

The technical assistance of Nadine Harmel and the financial support of the Deutsche Forschungsgemeinschaft (grant SFB470/C1 to SML and HB) is gratefully acknowledged. SVE thanks the Natural Sciences and Engineering Research Council of Canada for grant support and the Michael Smith Foundation for Health Research for the award of a Senior Scholarship.

References

Adams, P. D., Grosse-Kunstleve, R. W., Hung, L.-W., Ioerger, T. R., McCoy, A. J., Moriarty, N. W., Read, R. J., Sacchettini, J. C., Sauter, N. K. & Terwilliger, T. C. (2002). *Acta Cryst.* D**58**, 1948–1954.
Bowie, W. R., Caldwell, H. D., Jones, R. P., Mardh, P.-A., Ridgway, G. I. & Schachter, J. (1990). Editors. *Chlamydial Infections.* Cambridge University Press.
Britton, D. (1972). *Acta Cryst.* A**28**, 296–297.
Chandra, N., Acharya, K. R. & Moody, P. C. E. (1999). *Acta Cryst.* D**55**, 1750–1758.
Chook, Y. M., Lipscomb, W. N. & Ke, H. (1998). *Acta Cryst.* D**54**, 822–827.
Collaborative Computational Project, Number 4 (1994). *Acta Cryst.* D**50**, 760–763.
Declercq, J.-P. & Evrard, C. (2001). *Acta Cryst.* D**57**, 1829–1835.
Emsley, P. & Cowtan, K. (2004). *Acta Cryst.* D**60**, 2126–2132.
Essig, N. Z., Wood, J. F., Howard, A. J., Raag, G. & Whitlow, M. (1993). *J. Mol. Biol.* **234**, 897–901.
Frazão, C., Sieker, L., Coelho, R., Morais, J., Pacheco, I., Chen, L., LeGall, J., Dauter, Z., Wilson, K. & Carrondo, M. A. (1999). *Acta Cryst.* D**55**, 1465–1467.
Gomis-Rüth, F. X., Fita, I., Kiefersauer, R., Huber, R., Avilés, F. X. & Navaza, J. (1995). *Acta Cryst.* D**51**, 819–823.
Helliwell, M., Collison, D., John, G. H., May, I., Sarsfield, M. J., Sharrad, C. A. & Sutton, A. D. (2006). *Acta Cryst.* B**62**, 68–85.
Herbst-Irmer, R. & Sheldrick, G. M. (1998). *Acta Cryst.* B**54**, 443–449.
Kabat, E. A., Wu, T. T., Perry, H. M., Gottesman, K. S. & Foeller, C. (1991). *Sequences of Proteins of Immunological Interest*, 5th ed. Bethesda: National Institutes of Health.
Koch, E. (1992). *International Tables for Crystallography*, Vol. C, edited by A. J. C. Wilson, pp. 10–14. Dordrecht: Kluwer Academic Publishers.
Kosma, P. (1999). *Biochim. Biophys. Acta*, **1455**, 387–402.
Larsen, N. A., Heine, A., de Prada, P., Redwan, E.-R., Yeates, T. O., Landry, D. W. & Wilson, I. A. (2002). *Acta Cryst.* D**58**, 2055–2059.
Lebedev, A. A., Vagin, A. A. & Murshudov, G. N. (2006). *Acta Cryst.* D**62**, 83–95.
Lee, S., Sawaya, M. R. & Eisenberg, D. (2003). *Acta Cryst.* D**59**, 2191–2199.
Liang, J., Ealick, S., Nielsen, C., Schreiber, S. L. & Clardy, J. (1996). *Acta Cryst.* D**52**, 207–210.
MacRae, I. J. & Doudna, J. A. (2007). *Acta Cryst.* D**63**, 993–999.
Müller-Loennies, S., Gronow, S., Brade, L., MacKenzie, C. R., Kosma, P. & Brade, H. (2006). *Glycobiology*, **16**, 184–196.
Nguyen, H. P., Seto, N. O., MacKenzie, C. R., Brade, L., Kosma, P., Brade, H. & Evans, S. V. (2003). *Nature Struct. Biol.* **10**, 1019–1025.
Padilla, J. E. & Yeates, T. O. (2003). *Acta Cryst.* D**59**, 1124–1130.
Parsons, S. (2003). *Acta Cryst.* D**59**, 1995–2003.
Poulsen, J.-C. N., Harris, P., Jensen, K. F. & Larsen, S. (2001). *Acta Cryst.* D**57**, 1251–1259.
Rees, D. C. (1980). *Acta Cryst.* A**36**, 578–581.
Rees, D. C. & Lipscomb, W. N. (1980). *Proc. Natl Acad. Sci. USA*, **77**, 277–280.
Stanley, E. (1972). *J. Appl. Cryst.* **5**, 191–194.
Storoni, L. C., McCoy, A. J. & Read, R. J. (2004). *Acta Cryst.* D**60**, 432–438.
Wilson, A. J. C. (1949). *Acta Cryst.* **2**, 318–321.
Yeates, T. O. (1988). *Acta Cryst.* A**44**, 142–144.
Yeates, T. O. (1997). *Methods Enzymol.* **276**, 344–358.
Yeates, T. O. & Fam, B. C. (1999). *Structure Fold. Des.* **7**, R25–R29.
Zwart, P. H., Grosse-Kunstleve, R. W. & Adams, P. D. (2005). *CCP4 Newsl.* **42**, contribution 10.
Zwart, P. H., Grosse-Kunstleve, R. W., Lebedev, A. A., Murshudov, G. N. & Adams, P. D. (2008). *Acta Cryst.* D**64**, 99–107.